Electrophysiological Characterization of the Striatal Cholinergic Interneurons in *Dyt1 ΔGAG* Knock-In Mice

Hong Xing, Fumiaki Yokoi*, Ariel Luz Walker[†], Rosemarie Torres-Medina, Yuning Liu and Yuqing Li*

Department of Neurology, Norman Fixel Institute of Neurological Diseases, College of Medicine, University of Florida, Gainesville, FL, United States

DYT1 dystonia is an inherited early-onset movement disorder characterized by sustained muscle contractions causing twisting, repetitive movements, and abnormal postures. Most DYT1 patients have a heterozygous trinucleotide GAG deletion mutation (*ΔGAG*) in *DYT1/TOR1A,* coding for torsinA. *Dyt1* heterozygous ΔGAG knock-in (KI) mice show motor deficits and reduced striatal dopamine receptor 2 (D2R). Striatal cholinergic interneurons (ChIs) are essential in regulating striatal motor circuits. Multiple dystonia rodent models, including KI mice, show altered ChI firing and modulation. However, due to the errors in assigning KI mice, it is essential to replicate these findings in genetically confirmed KI mice. Here, we found irregular and decreased spontaneous firing frequency in the acute brain slices from *Dyt1* KI mice. Quinpirole, a D2R agonist, showed less inhibitory effect on the spontaneous ChI firing in *Dyt1* KI mice, suggesting decreased D2R function on the striatal ChIs. On the other hand, a muscarinic receptor agonist, muscarine, inhibited the ChI firing in both wild-type (WT) and *Dyt1* KI mice. Trihexyphenidyl, a muscarinic acetylcholine receptor M1 antagonist, had no significant effect on the firing. Moreover, the resting membrane property and functions of hyperpolarization-activated cyclic nucleotide-gated (HCN) channels, μ-opioid receptors, and large-conductance calcium-activated potassium (BK) channels were unaffected in *Dyt1* KI mice. The results suggest that the irregular and low-frequency firing and decreased D2R function are the main alterations of striatal ChIs in *Dyt1* KI mice. These results appear consistent with the reduced dopamine release and high striatal acetylcholine tone in the previous reports.

Keywords: dystonia, cholinergic interneuron, dopamine receptor, muscarine, μ-opioid receptor, quinpirole, trihexyphenidyl, torsinA

INTRODUCTION

Dystonia is a movement disorder with abnormal postures, twisting, and repetitive movements caused by sustained muscle contractions (1, 2). Dystonia can be caused by multiple etiologies, such as stroke, brain injury, sporadic, and gene alterations. DYT1 dystonia is an inherited movement disorder characterized by early-onset, generalized torsion, twisting, repetitive movements, or abnormal postures [DYT-TOR1A; Online Mendelian Inheritance in Man (OMIM) identifier #128100]. Most patients have a heterozygous in-frame trinucleotide deletion (ΔGAG) in *DYT1/TOR1A*, coding for torsinA (3). The penetrance is about 30%–40%, and non-symptomatic carriers of the *DYT1* gene mutation have an impairment in sequence learning (4, 5). Trihexyphenidyl (THP), an antagonist mainly to muscarinic acetylcholine receptor M1, ameliorates dystonic symptoms in DYT1 patients, suggesting a functional alteration in cholinergic or its related system (6, 7).

Two independent mutant mouse lines with the corresponding trinucleotide deletion in the endogenous *Dyt1/Tor1a* have been reported, i.e., the *Dyt1* ΔGAG heterozygous knock-in (KI) mice (www.informatics.jax.org; Allele Symbol: Tor1a^tm1Yql) (8) and *Tor1a*^{+/Δgag} KI mice (Tor1a^tm2Wtd) (9). Although both lines do not show overt dystonic symptoms, motor deficits of the hind limbs in the beam-walking test were reproduced in distinct batches of one line (8, 10, 11) and another line (12, 13). The same motor deficits in the beam-walking test were observed in other genetic dystonia mouse models, such as DYT11 myoclonus-dystonia and DYT12 rapid-onset dystonia with parkinsonism (14, 15), suggesting beam-walking deficits as a typical motor phenotype in these genetic dystonia mouse models. Motor deficits using other behavioral tests were also reported in other genetic animal models (16–19), such as rat (20), nematode (11), and fruit fly (21, 22). *Dyt1* KI mice exhibit the corticostriatal long-term depression (LTD) deficits (23), sustained contraction and co-contraction of agonist and antagonist muscles of hind limbs (24), motor deficits in the beam-walking test (8), and impaired motor-skill transfer (25). These phenotypes are ameliorated by trihexyphenidyl (THP) (23, 24, 26), suggesting that these phenotypes are caused by the same mechanism as DYT1 dystonia patients.

The fibroblasts from DYT1 patients show a reduction of torsinA (9). The mutant torsinA is quickly degraded in transfected cells, suggesting that the GAG deletion causes partial loss of torsinA function (27, 28). Both *Dyt1* knockdown mice (29) and *Dyt1* heterozygous KO mice (30) show motor deficits in the beam-walking test, suggesting that partial loss of torsinA contributes to the motor deficits. Both cerebral cortex-specific *Dyt1* conditional knockout (KO) mice (31), which were produced by crossing *Dyt1 loxP* mice and *Emx1-Cre mice* (32), and striatum-specific *Dyt1* conditional KO mice (33), which were produced by crossing *Dyt1 loxP* mice and *Rgs9-Cre mice* (34), also show beam-walking deficits (31). Therefore, the loss of torsinA function in the corticostriatal pathway contributes to motor deficits. Moreover, both cholinergic neuron-specific torsinA knockout (ChKO) mice with *Neo*

cassette (35) and those without *Neo* cassette (Ch2KO) mice show motor deficits (36). Dopamine receptor 2 (D2R)-expressing-cell-specific *Dyt1* conditional KO (d2KO) mice also show beam-walking deficits (37). On the other hand, the cerebellar Purkinje cell-specific *Dyt1* conditional KO and dopamine receptor 1 (D1R)-expressing-cell-specific *Dyt1* conditional KO (d1KO) mice show better performance in beam-walking (38). On the other hand, acute suppression of torsinA expression *via* AAV-TorsinA shRNA-GFP induces a dystonia-like phenotype (39), highlighting the contribution of the cerebellum to the pathogenesis of DYT1 dystonia (40). *Dyt1* KI mice show striatal D1R (25) and D2R reductions (23). *Dyt1* sKO and *Dyt1* d2KO mice show striatal D2R reduction and *Dyt1* d1KO mice show striatal D1R maturation deficits, suggesting that the D1R and D2R reductions are intrinsic cellular properties caused by the loss of torsinA in the corresponding neurons. *Dyt1* ΔGAG homozygous KI and *Dyt1* homozygous KO mice show neonatal lethality (8, 9, 31). On the other hand, the mutant mice with a combination of neuron- and glia-cell-specific *Dyt1* conditional KO and heterozygous KO show growth retardation and infant lethality, which can be rescued by enhanced care (41, 42).

Both *Dyt1* KI and heterozygous KO mice show similar hippocampal neurotransmitter releasing deficits (30, 43). *Tor1a*^{+/Δgag} KI mice show abnormal synaptic vesicle recycling, glutamate release, and calcium dynamics (44–46). Moreover, Dlx-CKO mice, which have a combination of forebrain-specific conditional KO of torsinA in one allele and heterozygous KO in the other allele, show neurodegeneration of the striatal ChIs, and the surviving ChIs showed a trend of reduced spontaneous firing (47). Transgenic hMT mice (48), transgenic ΔETorA rats (20), and "*Tor1a*^{+/Δgag} KI mice" (49) show abnormal ChI firing properties. However, it should be noted that "*Tor1a*^{+/Δgag} KI mice" in the paper were purchased from Jackson Lab (Stock No. 006251), which is *Tor1a*^{+/−} heterozygous KO mice lacking exons 2–4. Another recent report showed enhanced functions of μ-opioid receptors and large-conductance calcium-activated potassium (BK) channels of the striatal ChIs in *Tor1a* heterozygous KO mice (50).

Striatal ChIs show autonomous firing rather than reflections from the various synaptic input (51). The spontaneous firing patterns are affected by intrinsic membrane properties and the selective coupling of calcium currents to calcium-activated potassium currents and calcium dynamics (52–54). However, recent studies suggest that the striatal ChIs receive inputs from multiple neurons, including the cortical and the thalamic neurons (55) and the striatal medium spiny neurons (MSNs) (56–59). The striatal ChIs have an autofeedback mechanism through the inhibitory muscarinic acetylcholine receptors M2/M4 and RGS4 pathway (60, 61). Muscarine, a muscarinic acetylcholine receptor agonist, inhibits the striatal ChI firing in the rat brain slices by reducing N-, P- and L-type Ca^{2+} currents (62). Striatal ChIs affect the corticostriatal plasticity of the striatal MSNs (63). M1 and M4 muscarinic acetylcholine receptor mRNAs are expressed at high levels by the striatal MSNs (64) and have subtle changes in *Tor1a*^{+/Δgag} KI mice (65). The released ACh binds M1-type receptors and depolarizes the MSNs. ACh also

binds to M4 receptors on the direct pathway MSNs and modulates their activity (66). Moreover, striatal ACh binds to nicotinic acetylcholine receptors on the axons of dopaminergic neurons projecting from the substantia nigra pars compacta and synchronously stimulates local dopamine release (67). The released dopamine stimulates the surrounding D1R and D2R on the MSNs and D2R on the ChIs (57, 68).

Here, the striatal ChIs in the *Dyt1* KI mice were characterized by electrophysiological recording of acute brain slices and a cellular morphological approach. The spontaneous firing of striatal ChIs and its modulation by muscarine (muscarinic acetylcholine receptor agonist), quinpirole (D2R agonist), and THP (M1 receptor antagonist) were examined. Furthermore, the effect of DAMGO (μ-opioid receptor agonist) and PAX (BK channel blocker) on the membrane currents was investigated (50). Moreover, the resting membrane property, the intrinsic excitability and hyperpolarization-activated cyclic nucleotide-gated (HCN) channels of the striatal ChIs were measured. Finally, the dendritic structure and soma size of the recorded ChIs were quantified.

MATERIALS AND METHODS

Animals

All experiments were carried out in compliance with the USPHS Guide for Care and Use of Laboratory Animals and approved by the Institutional Animal Care and Use Committees of the University of Florida. *Dyt1* KI mice (Tor1a^{tm1Yql}) and their littermate WT mice were prepared and genotyped by PCR (8, 69). Since male *Dyt1* KI mice exhibited significant motor deficits in the previous study (8), only males were used for the present experiments. Mice were housed under a 12 h light and 12 h dark cycle with *ad libitum* access to food and water. All experiments were performed by investigators blind to the genotypes. This study followed the recommended heterogenization of study samples of various ages, and the data were analyzed with age as a covariate (70).

Brain Slices

Electrophysiological recordings for spontaneous firing and evoked firing of the striatal ChIs were obtained from 25 WT and 25 KI littermate male mice (6–11 weeks old), as described previously (71, 72).

Mice were anesthetized by the inhalation of isoflurane and decapitated. The brains were rapidly removed and briefly chilled in the ice-cold cutting solution containing (in mM) 190 Sucrose, 2.5 KCl, 1.25 NaH$_2$PO$_4$, 25 NaHCO$_3$, 1 CaCl$_2$, 10 MgCl$_2$, and 10 D-glucose and was oxygenated with 95% O$_2$–5% CO$_2$ (pH 7.35–7.45). In the same ice-cold cutting solution, coronal brain slices (300 μm-thick) were obtained with a Vibratome (LEICA VT 1000S, Leica Microsystems, Wetzlar, Germany). Slices were first incubated on a brain slice keeper (AutoMate Scientific, Inc. Berkeley, CA) with a thin layer of artificial cerebrospinal fluid (ACSF) containing (in mM) 127 NaCl, 2.5 KCl, 1.25 NaH$_2$PO$_4$, 25 NaHCO$_3$, 2 CaCl$_2$, 5 MgCl$_2$, and 10 D-glucose, saturated with 95% O$_2$ and 5% CO$_2$ (pH 7.35–7.45)

at 35°C for 60 min, followed by incubation at room temperature. After a minimum of 60-min incubation, each slice was transferred to a submerged recording chamber with the continuous flow (2 ml/min) of ACSF containing (in mM) 127 NaCl, 2.5 KCl, 1.25 NaH$_2$PO$_4$, 25 NaHCO$_3$, 2 CaCl$_2$, 1 MgCl$_2$, and 10 D-glucose and was constantly oxygenated with 95% O$_2$ and 5% CO$_2$ (pH 7.35–7.45). All experiments were carried out at 32 ± 0.5°C by a dual automatic temperature controller (TC-344B, Harvard Apparatus) under visual guidance using an inverted microscope equipped with infrared differential interference contrast (IR-DIC) videomicroscopy (Axioskop-FS; Carl Zeiss, Jena, Germany) and a 40× water-immersion lens.

Cell-Attached Recordings

The large neurons with ellipsoid-like soma were selected in the dorsal striatum under the microscope for the electrophysiological recordings. ChIs are further identified by whole-cell recording with step-current injection (73) and, in some cases, by a post hoc immunohistochemistry with an anti-ChAT antibody (71). Patch electrodes had a resistance of 5–10 MΩ when filled with a K-gluconate-based solution containing the following intracellular solution containing (in mM): 112.5 K-gluconate, 4 NaCl, 17.5 KCl, 0.5 CaCl$_2$, 1 MgCl$_2$, 5 K$_2$ATP, 1 NaGTP, 5 EGTA, 10 HEPES, pH 7.2 (270–280 mOsm/l). Biocytin (0.1%) was added to the recording electrode solution to allow post hoc immunohistochemical identification of the recorded cells. While approaching the cell, positive pressure was applied to the patch electrode. The seal (>5 GΩ) between the recording pipette and the cell membrane was obtained by suctioning the electrode. Action potential currents were recorded in the voltage-clamp mode, maintaining an average of 0 pA holding current. After baseline recording, some ChIs were investigated further with bath applications of muscarine [(+)-Muscarine chloride (Sigma Aldrich, M6532-5MG), 10 μM, 90 s (s)] or, THP [DL-Trihexyphenidyl hydrochloride (Sigma Aldrich, T1516-5G), 5 μM, 90 s)] for testing the effect of agonist and antagonist to the muscarinic acetylcholine receptors on the ChIs, respectively. Moreover, some other ChIs were investigated with bath applications of quinpirole [Quinpirole hydrochloride (Sigma Aldrich, Q102-25MG), 10 μM, 2 min] for testing the effect of the agonist to D2R on the ChIs. The effect of quinpirole on spontaneous firing was also examined in a different condition., the spontaneous firing was recorded for 30 s just before adding the drug into the recording bath. The drug was added for 90 s, and recording data in the last 30 s during the drug treatment period were used as "after treatment". In another condition, the firing was recorded for 3 min at around 10 min after starting the cell-attached recording. Ten μM quinpirole was then applied into the recording chamber for 3 min, followed by a 2 min wash out with ACSF and 3 min recording.

Whole-Cell Recording of the Striatal ChIs

Whole-cell recordings were made by breaking through the membrane. The electrophysiological intrinsic membrane properties (capacitance, input resistance, and time constant) were measured while holding the membrane potential at −60 mV. The liquid junction potential was compensated.

Electrode access resistances during all whole-cell recordings were maintained at <25 MΩ. The current steps were injected in multiple 200 pA from −0.8 to 0.6 nA, and the evoked-action-potentials were recorded in the whole-cell recording mode with the current clamp.

To further characterize the electrophysiological properties of μ-opioid receptors and BK channels of the striatal ChIs in *Dyt1* KI (*n* = 5) and control WT littermate male mice (*n* = 4) at 13–21 weeks-old, the current-voltage relationship of the striatal ChIs was measured by whole-cell recording mode during the voltage ramp (50) with the glass recording electrode filled with a K-gluconate solution containing the following (in mM): 125 K-gluconate, 0.5 EGTA, 19 HEPES, 0.3 GTP, 1 Mg-ATP, 10 NaCl, 2 $MgCl_2$, 1 $CaCl_2$. The brain slices were prepared as described above and incubated until recording. Each slice was transferred to a submerged recording chamber with the continuous flow (2 ml/min) of ACSF. The dorsal striatal ChIs were identified from their shape, and the spontaneous firing was confirmed in cell-attached mode, and then the membrane current was recorded in whole-cell recording mode. The membrane potential was held at −70 mV with a voltage clamp. The voltage ramp was applied from −60 to −140 mV in 500 ms, and the membrane current was recorded during the ramp. After multiple recordings, voltage ramp protocols were repeated when the recorded neurons were exposed to 1 μM tetrodotoxin (TTX), 1 μM TTX + 1 μM D-Ala2-MePhe4-Gly[ol]5enkephaline (DAMGO; AdipoGen; AG-CP3-0005V-M005), 1 μM TTX + 1 μM DAMGO + 1 μM Paxilline (PAX; Alomone labs; P-450) sequentially.

Recording Data Analysis

The recording data were acquired using pClamp 10 software and further analyzed by Mini Analysis Program (Synaptosoft). Signals were filtered at 5 kHz, and digitized at 10 kHz with a DigiData 1440 (Molecular Devices). Investigators who were blind to the genotypes performed the electrophysiological recordings and analysis. The 30 s (s) before drug treatment and the last 30 s during the drug treatment were used to analyze the drug effect on the spontaneous firing. For the 10-min quinpirole recording analysis, the 3 min before quinpirole treatment and the 3 min after 2 min of quinpirole washout were quantified.

Double-Staining of the Recorded Striatal ChIs and Tracing of the Dendrites

Since the neurons were recorded with the internal solution containing 0.1% biocytin, the recorded neurons were stained with fluorescent-conjugated streptavidin through biocytin-streptavidin binding. After the recordings, the brain slices were fixed overnight with 4% paraformaldehyde in 0.1M phosphate buffer (PB; pH 7.3) and stored in 0.1M PB. The slices were rinsed twice with 0.5% Triton X-100 in 0.02M PB for 10 min and then incubated for 2 hours protected from light in 0.5% (v/v) Triton X-100, 1% (w/v) bovine serum albumin (BSA), 0.02M PB, 0.2% (v/v) streptavidin Alexa Fluor 594 conjugate (Life technologies, S11227). The slices were rinsed with 0.5% Triton X-100 in 0.02M PB twice for 5 min each and then 0.02M PB once. The slices were washed in 10 mM glycine/PBS three times 5 min each and blocked in 2% gelatin/PBS for 15 min, 10 mM glycine/PBS for 5 min, and 0.1% BSA/PBS for

5 min. The blocked slices were incubated in goat anti-ChAT antibody (EMD Millipore, AB144P; 1:100 dilution) in 1% BSA/PBS for 2 h and washed in 0.1% BSA/PBS six times 5 min each. The slices were then incubated with Alexa Fluor 488 donkey anti-goat IgG (H+L) (Invitrogen, A11055; 1:200 dilution) in 1% BSA/PBS for 2 h and washed in 0.1% BSA/PBS six times 5 min each. The slices were mounted on glass slides with Vectashield Hard Set mounting medium for fluorescence (Vector Lab Inc., H-1400) and stored at 4°C overnight. The double-positive cells were confirmed using a ZEISS Axiophot RZGF-1 microscope with 2.5× or ×20 Plan-NEOFLUAR objective lens and FITC filter for Alexa Fluor 488 and Texas Red filter for Alexa Fluor 594, respectively. The dendrites were stained with streptavidin Alexa Fluor 594 conjugate and digitized at ×40 magnification using MBF Bioscience Neurolucida 7 and NeuroExplorer software (MicroBrightFields Bioscience). Sholl analysis (74) was performed using ImageJ software (NIH). Representative images were also taken by Olympus IX81-DSU Spinning Disk Confocal Microscope with ×60 Water immersion objective lens, FITC filter for Alexa Fluor 488, and Texas Red filter for Alexa Fluor 594, respectively.

Statistics

The spontaneous firing frequency and the drug effects were analyzed by a linear mixed model (lme), generalized linear mixed model (glmmTMB), and emmeans program in R version 4.1.2 (R Foundation for Statistical Computing, Vienna, Austria) for the animal-based nested data, or SAS GENMOD Procedure GEE model. The distribution of the data was checked by R shapiro.test. The coefficient of variation (CV), which is defined by standard deviations (SD) of the interspike intervals (ISI) per mean ISI (73), was analyzed by a generalized linear mixed model (R glmer) for the animal-based nested SD of ISI in gamma distribution concerning the offset log mean ISI. The number of paradoxically-excited ChIs was analyzed by R fisher.test. Wilcoxon rank-sum exact test was performed by R wilcox.test.

Median and confidence interval was analyzed by R MedianCI. The resting membrane property and I_H current were analyzed by R lme with the animal-based nested data. The recording order per ChI was also used as a variable for I_H. The current-step-evoked firing was analyzed by the SAS GENMOD Procedure GEE model with a negative binomial distribution. The membrane currents produced by voltage ramps were analyzed by the SAS GENMOD with gamma distribution concerning age. The number of intersections in Sholl analysis and the soma size of the ChIs were analyzed by Student's t-test (75). The length of the longest traced dendrites was analyzed by glmmTMB. Significance was assigned at $p < 0.05$.

RESULTS

Decreased Spontaneous Firing Frequency and Increased CV of the Striatal ChIs in *Dyt1* KI Mice

The striatal ChIs play a vital role in the pathogenesis of dystonia (76). The striatal ChIs in the *Dyt1* KI mice were

FIGURE 1 | Spontaneous firing of the striatal ChIs in the acute brain slices. **(A)** The representative traces of the striatal ChIs. Spontaneous firing frequency **(B)** significantly decreased, and CV **(C)** significantly increased in *Dyt1* KI mice. The bars represent means ± standard errors. The dots represent each data point. *p < 0.05.
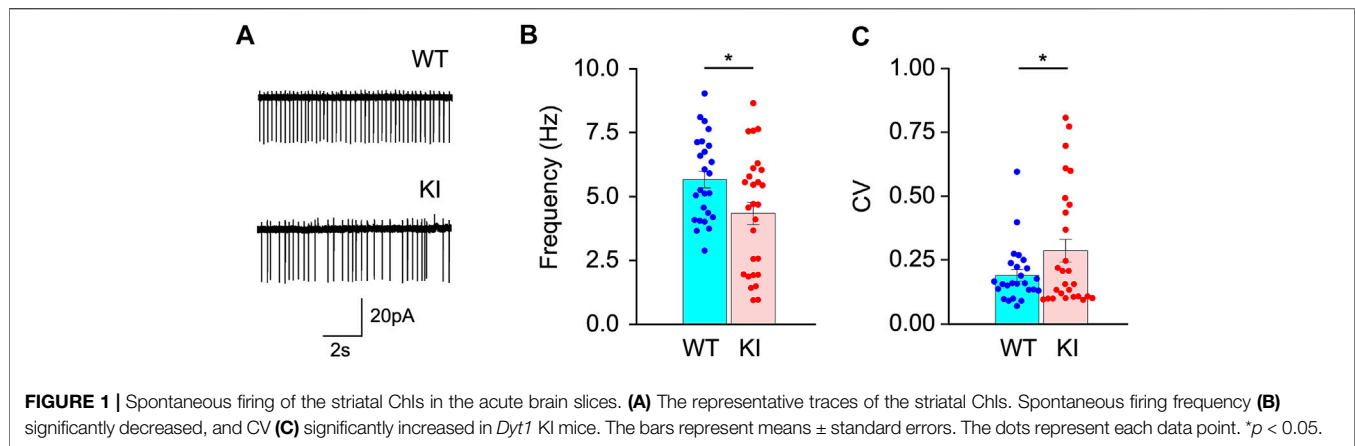
characterized by the electrophysiological recording of acute brain slices. The spontaneous firing of the striatal ChIs was recorded by cell-attached recording mode with a voltage clamp (WT, 25 cells/14 mice; KI, 27 cells/15 mice). As shown in the representative traces of the striatal ChIs (**Figure 1A**), the firing frequency was significantly decreased in *Dyt1* KI mice compared to WT mice [mean ± standard errors Hz; WT, 5.7 ± 0.3; KI, 4.3 ± 0.4; t(DF: 27) = −2.17, *p* = 0.039; **Figure 1B**]. *Dyt1* KI mice also showed significantly increased CV [WT, 0.19 ± 0.02; KI, 0.29 ± 0.04; t(27) = 2.02, *p* = 0.044; **Figure 1C**]. Increased CV suggests a high irregularity of firing.
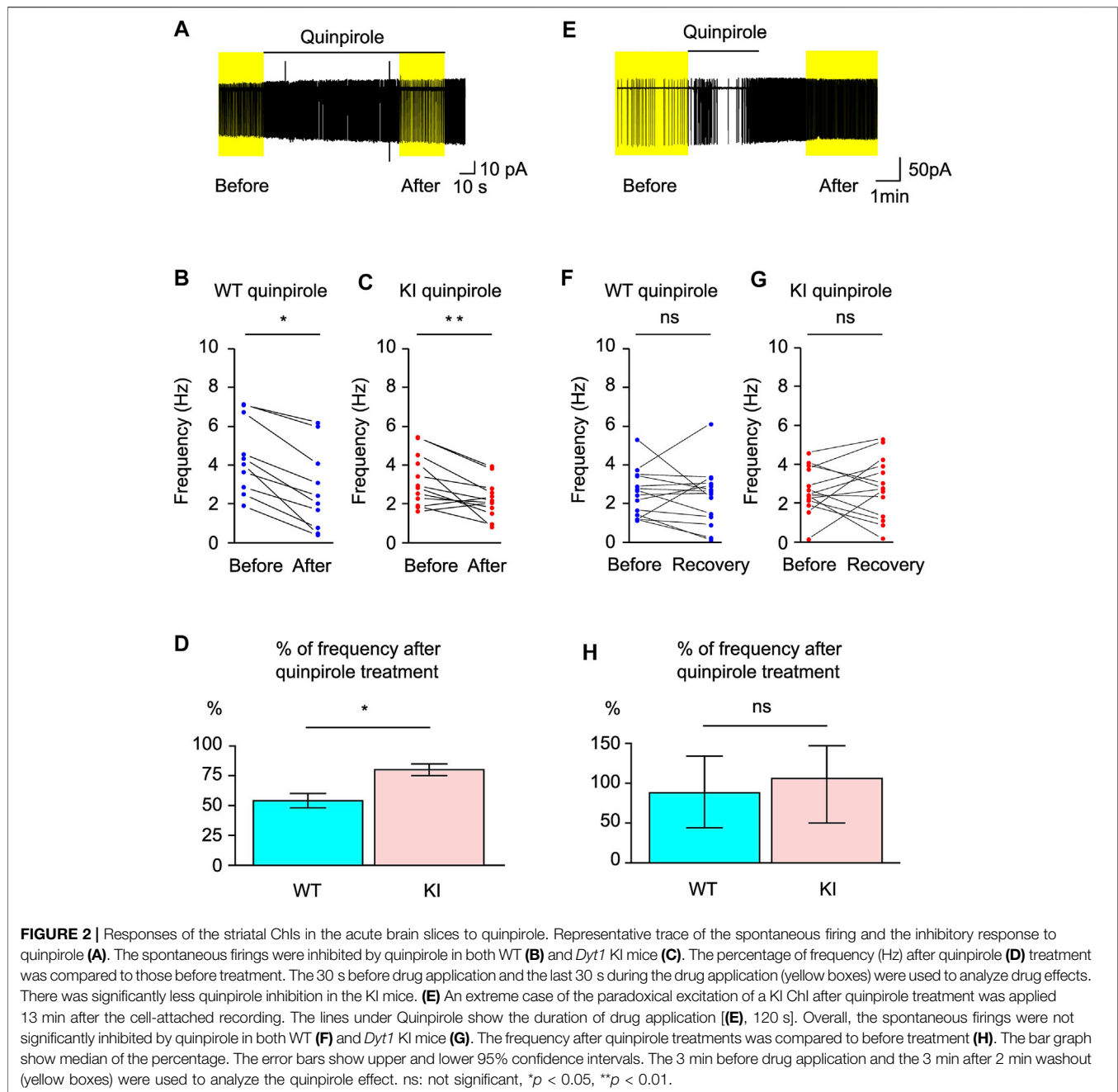
Less Inhibitory Effect of Quinpirole on the Firing of the Striatal ChIs in *Dyt1* KI Mice

D2R is reduced in the striatum of KI mice (23), but it is not known whether it is specifically reduced in striatal ChIs or not. The effect of quinpirole, a D2R agonist, on the spontaneous firing of striatal ChIs was further analyzed (WT, 10 cells/6 mice; KI, 12 cells/6 mice). A representative trace is shown in **Figure 2A**. The firing frequencies were decreased by quinpirole in both WT [Hz; before, 4.4 ± 0.8; after, 2.6 ± 0.8; t(13) = −2.9, *p* = 0.014; **Figure 2B**] and *Dyt1* KI mice [Hz; before, 3.2 ± 0.4; after, 2.2 ± 0.4; t(17) = −3.0, *p* = 0.0087; **Figure 2C**]. After the quinpirole application, the recording chamber solution was changed to ACSF for more than 2 minutes. Most ChIs showed recovery of the spontaneous action potentials in both WT and *Dyt1* KI mice. To compare the quinpirole inhibitory effect, we divided the frequency after the treatment by that before. Quinpirole showed less inhibitory effect in *Dyt1* KI mice compared to WT mice [WT, 54 ± 6%; KI, 80 ± 5%; Chi-Square (1) = 4.47, *p* = 0.034; **Figure 2D**]. Since the inhibitory D2R is expressed on the striatal ChIs, the results suggest that the inhibition through D2R may be less effective in *Dyt1* KI mice. As shown in **Figures 2B,C**, none of the ten ChIs in WT mice and two out of twelve ChIs in *Dyt1* KI mice showed paradoxical excitation, which is a reversed excitatory response to quinpirole. Although paradoxically-excited ChIs were observed only in *Dyt1* KI mice, Fisher's exact test showed no statistically significant difference in the number of

paradoxically-excited ChIs between WT and *Dyt1* KI mice (*p* = 0.48). On the other hand, there was no significant difference in the CV after the quinpirole treatment in WT (before, 0.30 ± 0.07; after, 0.34 ± 0.08; z = 0.70, *p* = 0.49) and *Dyt1* KI mice (before, 0.33 ± 0.07; after, 0.42 ± 0.09; z = 0.88, *p* = 0.38). Moreover, there was no significant difference between WT and *Dyt1* KI mice in the effect of quinpirole on the CV (WT, 125 ± 20%; KI, 146 ± 34%; z = 0.60, *p* = 0.55).

No Significant Difference in the Paradoxical Excitation of Striatal ChIs Between WT and *Dyt1* KI Mice After Quinpirole Treatment

Paradoxical activation of D2R by quinpirole was reported in several mouse and rat models of DYT1 dystonia (77–79). However, the paradoxical activation was not reproduced as detailed above. These published studies examined the quinpirole effect after extended baseline recording. Therefore we repeated the quinpirole experiment to mimic their recording condition. The firing frequency was compared before and after quinpirole treatment (WT, 14 cells/7 mice; KI, 14 cells/8 mice). The representative traces are shown in **Figure 2E**. There was no significant long-term effect of quinpirole on the firing frequencies in both WT [Hz; before, 2.6 ± 0.4; after, 2.4 ± 0.4; t(20) = −0.37 *p* = 0.72; **Figure 2F**] and *Dyt1* KI mice [Hz; before, 2.6 ± 0.4; after, 2.8 ± 0.4; t(20) = 0.31, *p* = 0.76; **Figure 2G**]. As shown in **Figures 2F,G**, five out of fourteen ChIs in WT mice and seven out of fourteen ChIs in *Dyt1* KI mice showed increased frequency compared to those before quinpirole treatment, which would qualify as paradoxical excitation. Fisher's exact test showed no significant difference in the number of paradoxically-excited ChIs between WT and *Dyt1* KI mice (*p* = 0.70). These results suggest no significant difference in the appearance of paradoxical excitation cells between the genotypes. The frequency after the treatment was divided by that before the treatment. Shapiro test showed that the ratio data were not normally distributed (WT, *p* = 0.030; KI, *p* = 1.7×10^{-6}; all, *p* = 5.6×10^{-10}). Wilcoxon rank-sum exact test showed that there was no significant difference in the long-term effect of quinpirole between WT and *Dyt1* KI mice [median, (lower,
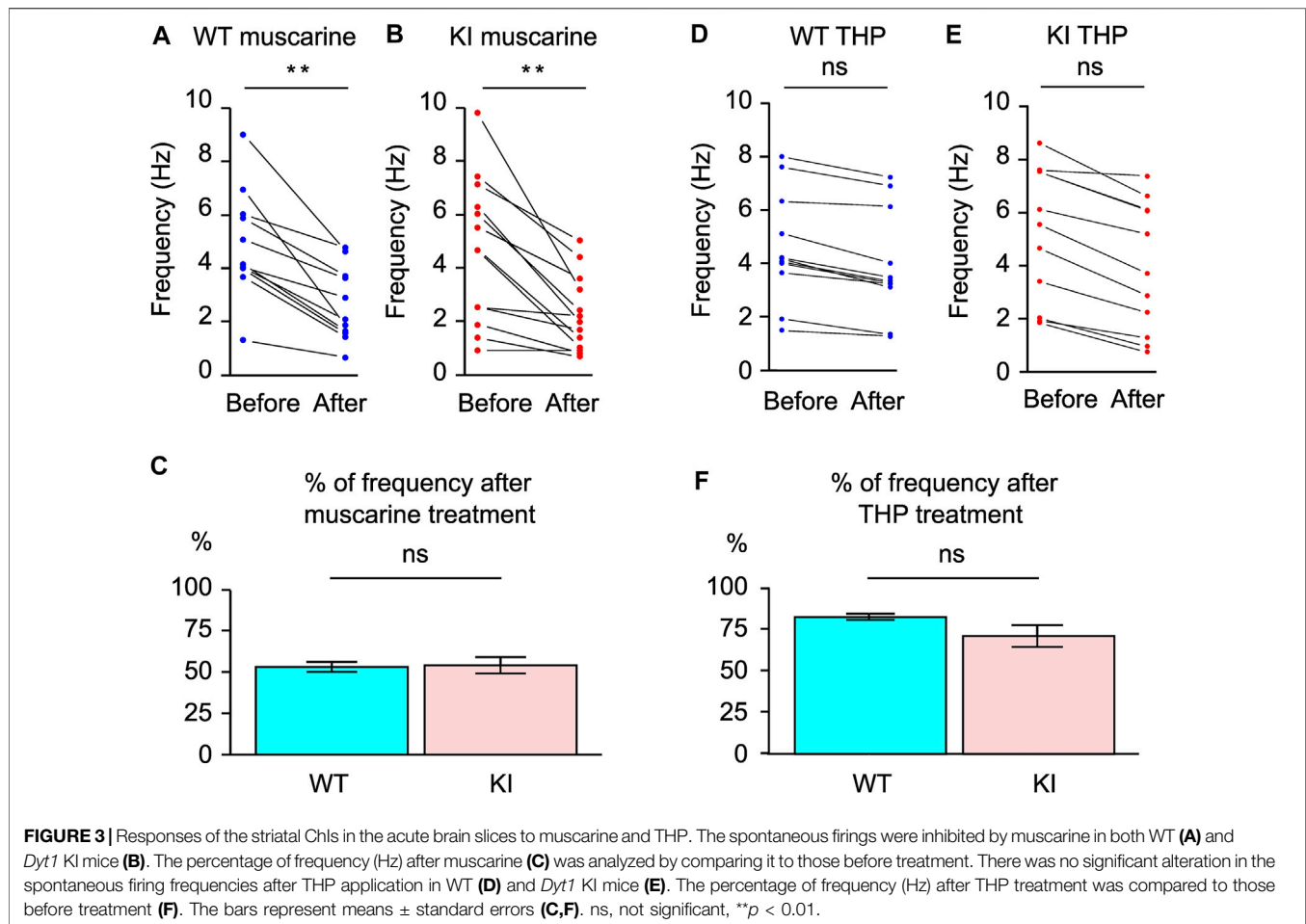
FIGURE 2 | Responses of the striatal ChIs in the acute brain slices to quinpirole. Representative trace of the spontaneous firing and the inhibitory response to quinpirole **(A)**. The spontaneous firings were inhibited by quinpirole in both WT **(B)** and *Dyt1* KI mice **(C)**. The percentage of frequency (Hz) after quinpirole **(D)** treatment was compared to those before treatment. The 30 s before drug application and the last 30 s during the drug application (yellow boxes) were used to analyze drug effects. There was significantly less quinpirole inhibition in the KI mice. **(E)** An extreme case of the paradoxical excitation of a KI ChI after quinpirole treatment was applied 13 min after the cell-attached recording. The lines under Quinpirole show the duration of drug application [**(E)**, 120 s]. Overall, the spontaneous firings were not significantly inhibited by quinpirole in both WT **(F)** and *Dyt1* KI mice **(G)**. The frequency after quinpirole treatments was compared to before treatment **(H)**. The bar graph show median of the percentage. The error bars show upper and lower 95% confidence intervals. The 3 min before drug application and the 3 min after 2 min washout (yellow boxes) were used to analyze the quinpirole effect. ns: not significant, *$p < 0.05$, **$p < 0.01$.

upper 95% confidence interval); WT, 88, (44, 134); KI, 106, (50, 147); W = 111, $p = 0.57$; **Figure 2H**].

Equivalent Inhibitory Effect of Muscarine on the Firing of the Striatal ChIs Between WT and *Dyt*1 KI Mice

Muscarine, a muscarinic acetylcholine receptor agonist, inhibits the striatal ChI firing, and this effect was found to be absent in ChKO mice (35) but was found to be normal Ch2KO mice (36). The effect of muscarine on the spontaneous firing of striatal ChIs in KI mice has not been examined and is explored here. We compared the firing before and after muscarine application (WT, 11 cells/6 mice; KI, 13 cells/ 6 mice). The firing frequencies were significantly decreased by muscarine in both WT [Hz; before, 4.9 ± 0.5; after, 2.6 ± 0.5; $t(15) = -3.15$, $p = 0.0066$; **Figure 3A**] and *Dyt1* KI mice [Hz; before, 4.6 ± 0.7; after, 2.2 ± 0.5; $z = -3.2$, $p = 0.0012$; **Figure 3B**]. To compare the inhibitory effect, we divided the frequency after the treatment by before the treatment. There was no significant difference in the inhibitory effect of muscarine between WT and *Dyt1* KI mice [WT, $53 \pm 3\%$; KI, $54 \pm 5\%$; Chi-Square (1) = 0.02, $p = 0.90$; **Figure 2C**]. Since inhibitory muscarinic acetylcholine receptors, M2/M4, are

FIGURE 3 | Responses of the striatal ChIs in the acute brain slices to muscarine and THP. The spontaneous firings were inhibited by muscarine in both WT **(A)** and *Dyt1* KI mice **(B)**. The percentage of frequency (Hz) after muscarine **(C)** was analyzed by comparing it to those before treatment. There was no significant alteration in the spontaneous firing frequencies after THP application in WT **(D)** and *Dyt1* KI mice **(E)**. The percentage of frequency (Hz) after THP treatment was compared to those before treatment **(F)**. The bars represent means ± standard errors **(C,F)**. ns, not significant, **$p < 0.01$.

expressed on the striatal ChIs, these results suggest that the inhibition through M2/M4 is not altered in *Dyt1* KI mice.

No Significant Effect of Trihexyphenidyl on the Firing of the Striatal ChIs in WT and *Dyt1* KI Mice

THP, a muscarinic acetylcholine receptor M1 antagonist, is effective in treating DYT1 patients and can reverse motor, electrophysiological, and EMG deficits in KI mice (23, 24, 26). The effect of THP on the spontaneous firing of striatal ChIs was examined to explore whether THP reverses the deficits by acting on striatal ChIs. We compared the firing before and after THP application (WT, 11 cells/3 mice; KI, 11 cells/ 4 mice). There was no significant alteration in the firing frequencies by THP in both WT [Hz; before, 4.6 ± 0.7; after, 3.8 ± 0.7; Chi-Square (1) = 2.76, $p = 0.097$; **Figure 3D**] and *Dyt1* KI mice [Hz; before, 5.5 ± 1.0; after, 4.1 ± 1.0; Chi-Square(1) = 3.74, $p = 0.053$; **Figure 3E**]. To compare the THP effect, we divided the frequency after the treatment by that of before and compared WT and *Dyt1* KI mice. There was no significant difference in the effect of THP between WT and *Dyt1* KI mice [WT, 83 ± 2%; KI, 71 ± 7%; Chi-Square(1) = 1.80, $p = 0.18$; **Figure 3F**]. These results

suggest that THP does not affect the spontaneous firing of the ChIs in KI mice.

No Significant Alteration in the Membrane Property and the Intrinsic Excitability of the Striatal ChIs in *Dyt1* KI Mice
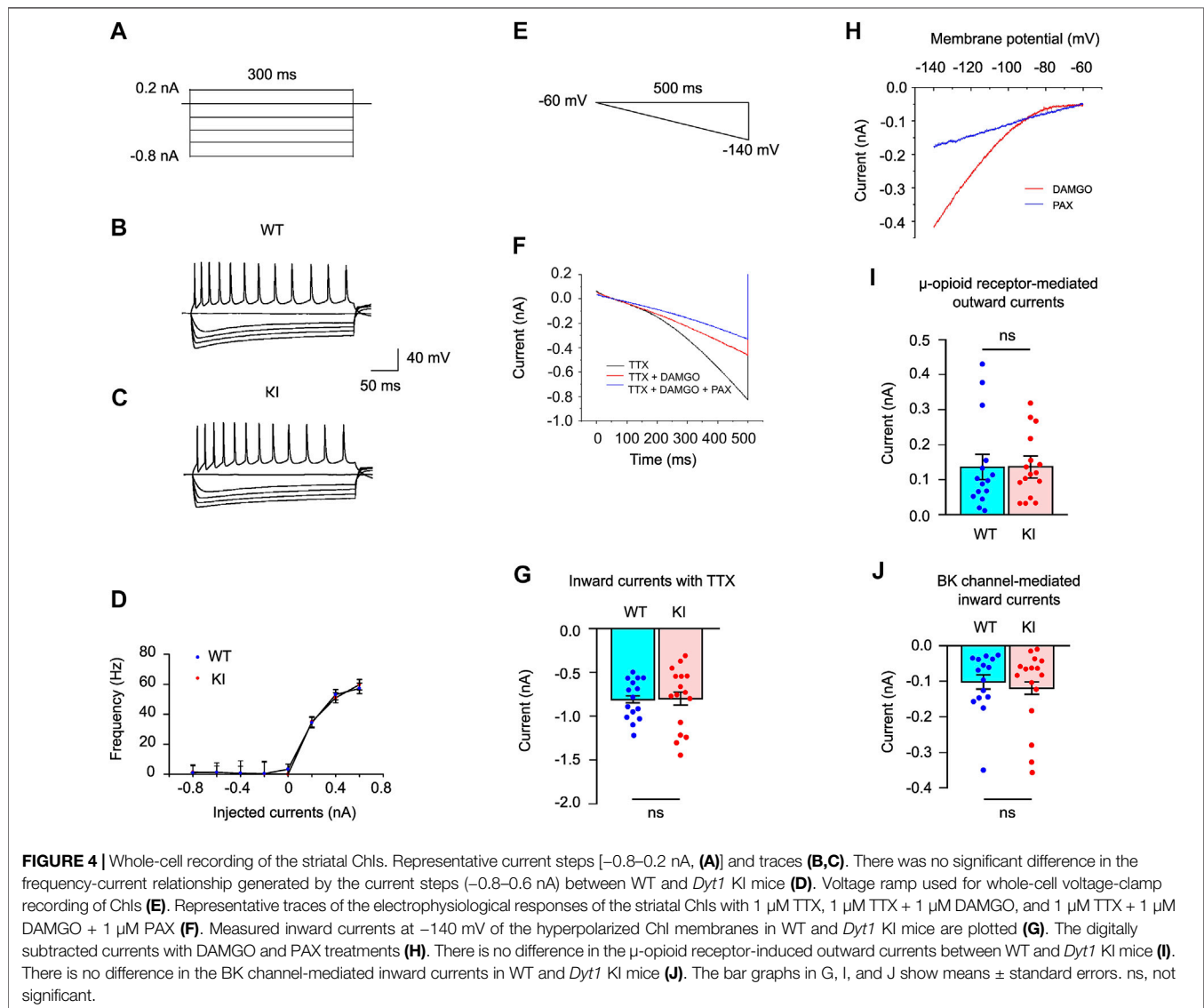
This series of experiments is to determine whether the membrane property and intrinsic excitability contribute to the reduced spontaneous firing of striatal ChIs in the KI mice or not. After recording the spontaneous firing by cell-attached mode, the intrinsic membrane properties were measured in whole-cell recording mode. The resting membrane property of the striatal ChIs was characterized in the brain slices from 11 WT (29 cells) and 15 *Dyt1* KI mice (26 cells). There was no significant difference in the resting membrane potential (RMP), the membrane capacitance, the input resistance (IR), or the time constant between WT and *Dyt1* KI mice (**Table 1**).

The intrinsic excitability of the striatal ChIs in the brain slices was measured with current step injections (**Figures 4A–C**). The recorded neurons showed typical electrophysiological properties of the striatal ChIs (51). The hyperpolarization and cyclic nucleotide activated cation current (I_H) was calculated (80). There was no significant alteration in I_H between WT and

TABLE 1 | Electrophysiological characterization of the ChI resting membrane property in the dorsal striatum.

	RMP (mV)	Capacitance (pF)	IR (MΩ)	Time Constant (ms)	I_H
WT	−61.2 ± 1.9	77.7 ± 5.0	150 ± 9.0	0.91 ± 0.08	20.6 ± 4.3
KI	−61.2 ± 1.9	75.1 ± 5.2	148 ± 9.3	0.91 ± 0.08	22.0 ± 4.6
t (DF)	−0.01 (8)	−0.37 (8)	−0.12 (8)	0.04 (8)	0.23 (17)
p	0.99	0.72	0.91	0.97	0.83

The resting membrane property was obtained from 5 WT (12 cells) and 5 Dyt1 KI, mice (11 cells). I_H, was obtained from one or two recordings per cell in 3 WT (14 recordings from 10 cells) and 3 Dyt1 KI mice (10 recordings from 9 cells). The p-value was calculated by R lme program with the animal-based nested data and the recording order per cell as a variable (for I_H). There was no significant difference between the first and the second recordings (p = 0.60 for I_H). The mean ± standard error was calculated by R emmeans program. RMP, resting membrane potential; IR, input resistance; I_H, hyperpolarization and cyclic nucleotide activated cation current; DF, degree of freedom.

FIGURE 4 | Whole-cell recording of the striatal ChIs. Representative current steps [−0.8–0.2 nA, **(A)**] and traces **(B,C)**. There was no significant difference in the frequency-current relationship generated by the current steps (−0.8–0.6 nA) between WT and *Dyt1* KI mice **(D)**. Voltage ramp used for whole-cell voltage-clamp recording of ChIs **(E)**. Representative traces of the electrophysiological responses of the striatal ChIs with 1 μM TTX, 1 μM TTX + 1 μM DAMGO, and 1 μM TTX + 1 μM DAMGO + 1 μM PAX **(F)**. Measured inward currents at −140 mV of the hyperpolarized ChI membranes in WT and *Dyt1* KI mice are plotted **(G)**. The digitally subtracted currents with DAMGO and PAX treatments **(H)**. There is no difference in the μ-opioid receptor-induced outward currents between WT and *Dyt1* KI mice **(I)**. There is no difference in the BK channel-mediated inward currents in WT and *Dyt1* KI mice **(J)**. The bar graphs in G, I, and J show means ± standard errors. ns, not significant.

Dyt1 KI mice (**Table 1**), suggesting that HCN channels were normal in *Dyt1* KI mice.

Moreover, the frequency-current relationship showed that there was no significant alteration in the firing frequencies between WT and *Dyt1* KI mice (0.2 nA injection; WT, 34.4 ± 3.5 Hz; KI, 35.0 ± 3.4 Hz; z = 0.32, p = 0.75; 0.4 nA injection; WT, 53.1 ± 3.4 Hz; KI, 51.0 ± 3.4 Hz; z = −0.97, p = 0.33; 0.6 nA injection; WT, 57.3 ± 3.5 Hz; KI, 59.8 ± 3.5 Hz; z = 0.46, p = 0.65; **Figure 4D**). These results suggest that the intrinsic excitability of the striatal ChIs is not altered in *Dyt1* KI mice.

No Significant Alteration in the Inward Currents Induced by Hyperpolarization of the Striatal ChIs in *Dyt1* KI Mice

Hyperpolarization of the membrane potential by voltage ramp induces an influx of cation ions through multiple voltage-gated ion channels and causes inward currents. Changes in opioid receptor signaling and BK channels have been reported in DYT1 mouse models (50). We decided to validate the findings in our KI mice. The membrane potential of the striatal ChIs was hyperpolarized by voltage ramp (-60 to -140 mV in 500 ms; **Figure 4E**) with 1 µM TTX (voltage-dependent Na$^+$ channel blocker) in the brain slices from 4 WT (15 cells) and 5 *Dyt1* KI mice (16 cells). The inward currents induced by the voltage ramp were recorded in whole-cell recording mode (**Figure 4F**). The recorded currents with TTX at -140 mV are shown in **Figure 4G**. There was no significant alteration in the inward currents with TTX between WT and *Dyt1* KI mice [WT, -0.81 ± 0.04 nA; KI, -0.80 ± 0.07 nA; $z = 0.12$, $p = 0.91$; **Figure 4G**], suggesting that the overall hyperpolarization-activated ion channel function is normal in *Dyt1* KI mice.

No Significant Alteration in the Striatal ChI Outward Currents Induced by Stimulation of µ-opioid Receptors in *Dyt1* KI Mice

Stimulation of µ-opioid receptors produces outward currents by inducing the outflux of potassium ions (K$^+$) and inhibiting the influx of calcium ions (Ca^{2+}) through the G-protein-coupling mechanism (81). DAMGO stimulates µ-opioid receptors and attenuates the inward currents (82). DAMGO (µ-opioid receptor agonist; 1 µM) was used to analyze the property of µ-opioid receptors during the voltage ramp (50). DAMGO attenuated the inward currents of the hyperpolarized ChI membranes in WT and *Dyt1* KI mice (**Figures 4E,F**). The DAMGO-induced outward currents were calculated by digital subtraction of the currents recorded with TTX and DAMGO from those with only TTX (**Figure 4H**). The currents recorded with TTX and DAMGO at -140 mV are shown in **Figure 4I**. There was no significant alteration in the µ-opioid receptor-induced outward currents between WT and *Dyt1* KI mice [WT, 0.14 ± 0.04 nA; KI, 0.14 ± 0.03 nA; $z = 0.0$, $p = 1.0$; **Figure 4I**], suggesting normal µ-opioid receptor function in *Dyt1* KI mice.

No Significant Alteration in the Striatal ChI Inward Current Through BK Channels in *Dyt1* KI Mice

The opening of multiple ion channels induces hyperpolarization-activated inward currents in this recording condition. Among the ion channels, the flow of potassium ions through the BK channel is bidirectional, depending on the membrane potential (83, 84). In the depolarized membrane potential, the opening of the BK channel produces an outflux of potassium ions (K$^+$). It causes outward currents during the falling phase of the action potential (85). When the membrane potential is hyperpolarized artificially by voltage ramp, the opening of the BK channel induces an influx of potassium ions (K$^+$), which causes inward currents. Therefore, blocking the BK channel attenuates the inward currents of the artificially hyperpolarized membrane potential.
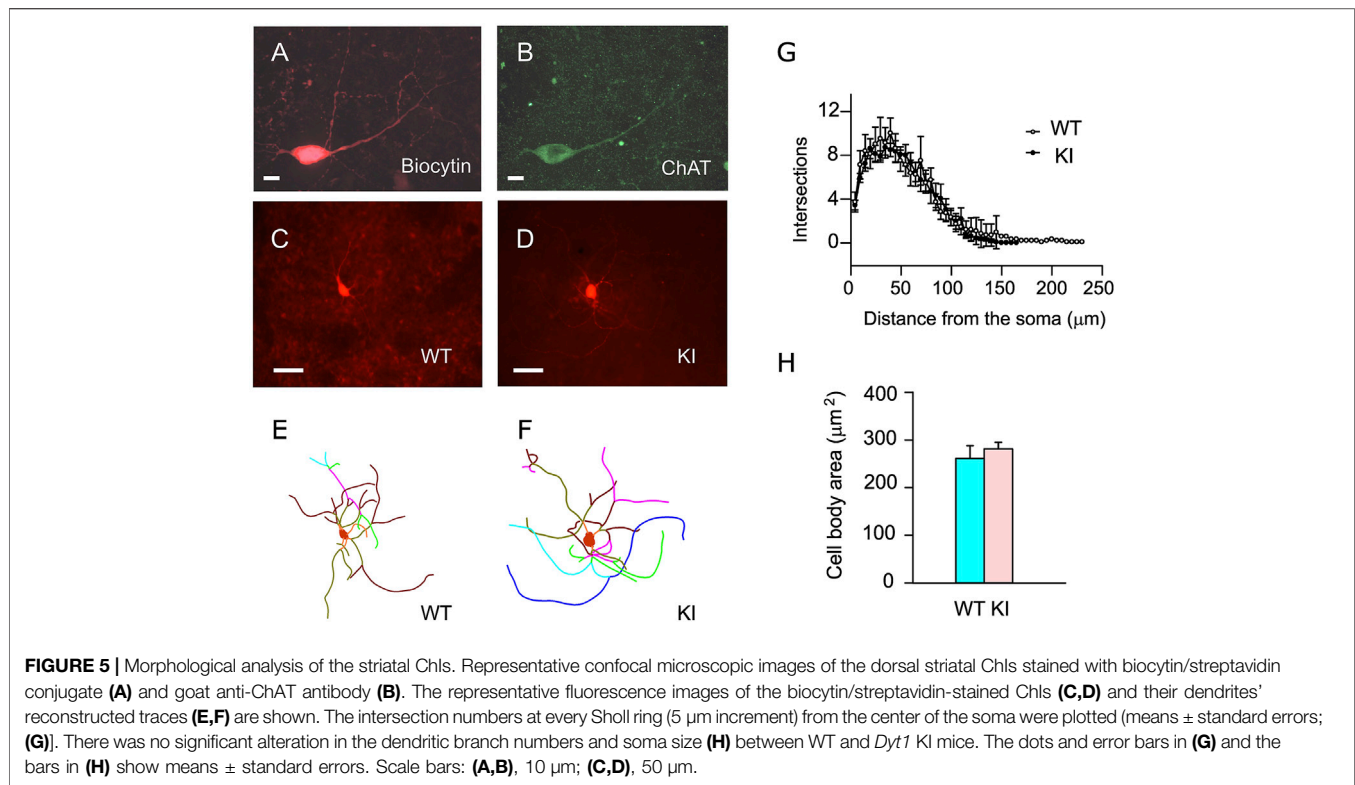
The BK channel activity was characterized by adding 1 µM PAX (BK channel blocker) during the voltage ramp. PAX blocked the BK channel and attenuated the BK-channel-derived inward currents (**Figures 4E,F**). The BK-channel-derived inward currents were calculated by digital subtraction of the currents recorded with TTX, DAMGO, and PAX from those with only TTX and DAMGO (**Figure 4H**). The currents recorded with TTX, DAMGO, and PAX at -140 mV are shown in **Figure 4J**. There was no significant alteration in the inward current through the BK channels between WT and *Dyt1* KI mice [WT, -0.10 ± 0.02 nA; KI, -0.12 ± 0.02 nA; $z = -0.65$, $p = 0.52$; **Figure 4J**], suggesting normal ChI BK-channel function in *Dyt1* KI mice.

No Significant Morphological Alteration in the Striatal ChI Dendrites in *Dyt1* KI Mice

The dendrite structures and soma size of the recorded ChIs were examined by Sholl analysis (74). The morphology of the ChI dendrites was analyzed by digital tracing. Dorsal striatal ChIs were filled with biocytin during the whole-cell patch-clamp recording and labeled with streptavidin Alexa Fluor 594 (**Figure 5A**). The brain slices were stained with goat anti-ChAT/anti-goat IgG Alexa Fluor 488 to verify cholinergic identity (**Figure 5B**). The representative dendrites of the striatal ChIs labeled with biocytin/streptavidin Alexa Fluor 594 (**Figures 5C,D**) and their digitized dendrites are shown (**Figures 5E,F**). The dendritic branch numbers in 8 ChIs from 6 WT mice and 17 ChIs from 10 *Dyt1* KI mice were quantified by Sholl analysis (74) and the ImageJ program (NIH). There was no significant alteration in the number of intersections between WT and *Dyt1* KI mice ($p > 0.05$ at each comparable data point; **Figure 5G**). Moreover, there was no significant alteration in the length of the longest traced dendrites between WT and *Dyt1* KI mice (length ± standard errors; WT: 125 ± 9 µm; KI: 116 ± 6 µm; $p = 0.38$; **Figure 5G**). There was no significant alteration in the soma size between WT and *Dyt1* KI mice (cell body area ± standard errors; WT: 261 ± 27 µm^2; KI: 281 ± 14 µm^2; $p = 0.47$; **Figure 5H**). The results suggest no significant morphological alteration in the striatal ChI dendrites between WT and *Dyt1* KI mice.

DISCUSSION

TorsinA has been shown to be involved in multiple cellular processes, including protein quality control and secretion, calcium homeostasis, nuclear envelope integrity, nucleo-cytoplasmic transport, nucleo-cytoskeletal coupling, lipid metabolism, and synaptic transmission and plasticity (86). TorsinA is likely a molecular chaperon that processes various proteins, including the maturation of striatal D2R (37, 77) and D1R (38). Heterozygous *Dyt1* KI mice, which have the corresponding mutation, show motor deficits and less reduced locomotor response to raclopride, a D2R antagonist. *Dyt1* KI

FIGURE 5 | Morphological analysis of the striatal ChIs. Representative confocal microscopic images of the dorsal striatal ChIs stained with biocytin/streptavidin conjugate **(A)** and goat anti-ChAT antibody **(B)**. The representative fluorescence images of the biocytin/streptavidin-stained ChIs **(C,D)** and their dendrites' reconstructed traces **(E,F)** are shown. The intersection numbers at every Sholl ring (5 μm increment) from the center of the soma were plotted (means ± standard errors; **(G)**]. There was no significant alteration in the dendritic branch numbers and soma size **(H)** between WT and *Dyt1* KI mice. The dots and error bars in **(G)** and the bars in **(H)** show means ± standard errors. Scale bars: **(A,B)**, 10 μm; **(C,D)**, 50 μm.

mice also show decreases in striatal D2R, D2R ligand binding, and torsinA levels. Since the striatal D2R reduction in *Dyt1* KI mice was mainly derived from the striatal indirect pathway medium spiny neurons (iMSNs), it was not known whether D2R function on striatal ChIs is reduced as well or not. Here, the striatal ChIs in acute brain slices showed irregular spontaneous firing with decreased frequency in *Dyt1* KI mice, whereas the intrinsic excitability was normal. Quinpirole, a D2R agonist, showed less inhibitory effect on the spontaneous ChI firing in *Dyt1* KI mice, suggesting decreased D2R function on the striatal ChIs. Muscarine, a muscarinic receptor agonist, inhibited the ChI firing in *Dyt1* KI mice, whereas trihexyphenidyl, a muscarinic acetylcholine receptor M1 antagonist, had no significant effect on the firing. Moreover, the resting membrane property, HCN channels, μ-opioid receptors, and BK channels of striatal ChIs were unchanged in *Dyt1* KI mice. These results suggest that the irregular and low-frequency firing and decreased D2R function are the main alterations of striatal ChIs in *Dyt1* KI mice. Consistent with the dystonic symptom caused by the side effect of D2R blockers, the striatal D2R defect on the striatal ChIs and iMSNs may contribute to the symptoms of DYT1 dystonia (13).

Paradoxical excitation to D2R activation was reported in several mouse and rat models of DYT1 dystonia (77-79, 87), *Thap1*[C54Y/+] knock-in mice (DYT6 dystonia model) and *Gnal*^{+/-} KO mice (DYT25 dystonia model) (87). We did not find such a difference between WT and *Dyt*1 KI mice in two separate quinpirole experiments. We found less inhibitory response during quinpirole treatment, in contrast to the paradoxical

excitation reported in the transgenic hMT mice (48), ChKO mice (35), transgenic ΔETorA rats (20), and *Tor1a*[+/Δgag] mice (49, 78, 79, 87). The mutations introduced in ChKO mice differ from the ΔGAG mutation commonly seen in most DYT1 dystonia patients and the *Dyt1* KI mice. Transgenic hMT mice and ΔETorA rats might have non-physiological levels of torsinA and ectopic expression of the exogenous mutant torsinA. Abnormal motor behaviors have been reported in overexpression mouse models of human WT and mutant *DYT1/TOR1A* gene (88), highlighting the importance of using *Dyt1* KI mice to study the pathophysiology of DYT1 dystonia (16). The discrepancy in paradoxical excitation between *Tor1a*[+/Δgag] mice and *Dyt1* KI mice is not known and could be attributed to the difference in KI mouse construction, animal husbandry, recording configuration, sample size, statistical analysis methods, and other unknown contributing factors.

Enhanced functions of μ-opioid receptors and large-conductance calcium-activated potassium (BK) channels of the striatal ChIs were found in *Tor1a* heterozygous KO mice (50). The authors were able to show similarly enhanced μ-opioid receptor function on the firing rate of striatal ChIs in *Tor1a*[+/Δgag] KI mice. We did not find any significant difference in the functions of μ-opioid receptors and BK channels in the *Dyt1* KI mice. Our results are consistent with the normal opioid binding in DYT1 patients (89). Since mutant torsinA still has low ATPase activity (90), which might be sufficient to maintain the normal function of μ-opioid receptors and BK channels in *Dyt1* KI mice.

Mechanisms to produce a low frequency of the ChI firing in *Dyt1* KI mice are not known. Here the intrinsic membrane property was normal in *Dyt1* KI mice. Moreover, the quinpirole showed a less inhibitory effect through D2R on the ChIs in *Dyt1* KI mice. These results suggest that the low frequency may be caused by a network effect rather than the intrinsic characteristic of the ChIs. Although striatal ChIs are pacemaker cells with spontaneous firing, they receive multiple inputs, including GABA from MSNs (56–59, 91). Since striatal D2R is decreased in *Dyt1* KI mice, the D2-expressing MSNs, i.e., iMSNs, may increase the firing probability of releasing GABA and suppress the ChIs. On the other hand, striatal D1R is also decreased in *Dyt1* KI mice. Therefore, the D1R-expressing MSNs, i.e., direct pathway medium spiny neurons (dMSNs), may reduce the release probability of GABA for suppressing the ChIs. Since the average ChI firing frequency is decreased in *Dyt1* KI mice, the increased GABA inputs from iMSNs seem more dominant than reduced GABA inputs from dMSNs. This may be consistent with the electron microscopic observations that 47% of the indirect pathway terminals and 36% of the direct pathway terminals of the GABAergic neurons target striatal ChIs in rhesus monkeys (92). Increased GABA inputs from other neurons may also decrease the ChI firing frequency in *Dyt1* KI mice; further characterization of GABAergic inputs to the ChIs, such as IPSCs, in *Dyt1* KI mice is needed to elucidate the mechanism of the low and irregular frequency of ChIs.

Since acetylcholine released from the ChIs synchronously stimulates striatal dopamine release (67), the low frequency of the ChIs may cause striatal dopamine release deficits in *Dyt1* KI mice. The basal level of striatal extracellular dopamine and amphetamine-stimulated dopamine release are consistently reduced in another KI mouse line of DYT1 dystonia (12). Suppression of the dopaminergic system is known to produce dystonic symptoms in humans. For example, dystonic symptoms are a well-known side effect of D2R antagonists used as antipsychotics (93). Dopamine synthesis deficits cause DYT5 dopa-responsive dystonia (94). The indirectly defected dopaminergic pathway may cause the dystonic symptoms in DYT1 dystonia.

Quinpirole showed a less inhibitory effect on the striatal ChIs in *Dyt1* KI mice, suggesting decreased D2R function on the ChIs. This is consistent with the previous reports of decreased striatal D2R protein level (23), reduced binding of D2R radioligand [^{3}H] YM-09151 to the striatum, and less reduced locomotor response to D2R antagonist raclopride in *Dyt1* KI mice (38). However, the measured striatal D2R protein level and D2R radioligand binding are mainly derived from the striatal iMSNs. TorsinA is a molecular chaperon that contributes to the trafficking of polytopic membrane-bound proteins, including G protein-coupled receptors (95). Moreover, *Dyt1* d2KO mice show striatal D2R maturation deficits (37). Since *Dyt*1 KI mice express decreased striatal torsinA levels (96), these results suggest that the partial loss of torsinA may reduce D2R in the ChIs as well as the iMSNs.

The mechanism of the irregular ChI firing or high CV in *Dyt1* KI mice is unknown. The decreased D2R function in the ChIs itself causes less inhibition by dopamine and contributes to an increased ChI firing frequency. Therefore, the ChIs may receive both the increased GABA release from iMSNs and less inhibitory signal by dopamine. Combining these opposing signals may cause the irregular frequency of the ChIs in the KI mice. Since *Dyt1* KI mice show irregular spontaneous firing in the cerebellar Purkinje cells (97), the heterozygous ΔGAG mutation seems to produce irregular firing in both ChIs and Purkinje cells. We found BK channel activity is increased in the KI Purkinje cells, which could underlie the irregular firing pattern (97). Here, we demonstrated no change of BK channel activity in the KI ChIs. The ionic mechanisms responsible for the altered ChI firing regularity remain to be investigated.

The spontaneous firing was inhibited by muscarine in WT and *Dyt1* KI mice, suggesting normal inhibitory function through M2 on the ChIs in *Dyt1* KI mice. The cholinergic neuron-specific torsinA knockout (Ch2KO) mice consistently show normal inhibitory responses (36). However, the striatal ChIs in cholinergic neuron-specific torsinA knockout (ChKO) mice with Neo cassette show no reaction to muscarine (35). The normal M2 function may also decrease the firing frequency of the ChIs if the striatal cholinergic tone is increased in the *Dyt1* KI mice, as shown in another line of KI mice (79). The mechanism to produce a high cholinergic tone is still not known. It may relate to the irregular firing of ChIs or the partial loss of ChIs in *Dyt1* KI mice (26). The irregular and low-frequency firing of striatal ChIs in *Dyt1* KI mice seems consistent with the high striatal acetylcholine tone in the previous reports (79). Further analysis of the striatal acetylcholine overflow mechanism will elucidate the pathophysiology of DYT1 dystonia.

The ChIs in both WT and *Dyt1* KI mice did not significantly respond to THP, consistent with the lack of expression of M1-type stimulatory muscarinic acetylcholine receptors on the striatal ChIs (98, 99). THP likely affected other neurons, such as MSNs in the corticostriatal pathway. *Dyt1* KI mice exhibit corticostriatal LTD deficits, abnormal muscle contraction, motor deficits, and impaired motor-skill transfer (8, 12, 23, 25, 100). These deficits are ameliorated by THP treatment (23, 24, 26), suggesting functional alteration of cholinergic or its related circuits in *Dyt1* KI mice. As discussed above, the decreased frequency of the ChIs may be caused indirectly by decreased D2R on iMSNs. MSNs project GABAergic axons to ChIs and inhibit the ChI firing. The iMSNs with decreased D2R may increase GABA release to ChIs and suppress the firing of the ChIs in *Dyt1* KI mice. THP may also intervene in this pathway and attenuate the symptoms by recovering the ChI firing. Further analysis of the network effect of these neurons will elucidate the contribution of each pathway to producing the motor deficits.

DYT1 dystonia is known as a circuit disorder rather than a neurodegenerative disorder. There is no overt neurodegeneration in DYT1 dystonia patients (1) and *Dyt1* KI mice (8). Consistently, cerebral cortex-specific *Dyt1* conditional KO mice do not show overt developmental alteration in cerebral cortex neurons (31). However, there is a slight morphological alteration in the cerebellar Purkinje cells in *Dyt1* KI mice and Purkinje cell-specific *Dyt1* conditional KO mice (101). The size of the

central nucleus of the amygdala is significantly reduced in the KI mice ([69](#)). Subtle morphological alterations in the cerebellar Purkinje cells were also reported in another line of KI mice ([102](#)). Moreover, the KI mice show a reduced ratio of axo-spinous to axo-dendritic synaptic inputs to MSNs from glutamatergic and dopaminergic sources ([103](#)). We found no significant alteration in dendritic branch numbers, suggesting that local connection with the striatal ChIs is mostly normal in *Dyt1* KI mice. Since the striatal ChIs show abnormal firing patterns, the electrophysiological alteration may not be caused by overt local neuronal connection changes. However, *Dyt1* KI mice have a slightly decreased number of dorsolateral striatal ChIs ([26](#)). The normal dendrite of the examined striatal ChIs does not exclude the possibility that a few ChIs with abnormal structure were already degenerated or eliminated during the development. The relationship between functional alteration and neuronal connections remains to be further examined.

DATA AVAILABILITY STATEMENT

The datasets presented in this article are not readily available because of the lack of a public electrophysiological data depository. Requests to access the datasets should be directed to the corresponding authors.

ETHICS STATEMENT

The animal study was reviewed and approved by the Institutional Animal Care and Use Committees of the University of Florida.

AUTHOR CONTRIBUTIONS

HX, FY, and YLi designed the experiments. HX, FY, AW, RT-M, and YLu performed the experiments. HX, FY, AW, and YLI analyzed the data. FY wrote the manuscript. HX, AW, and YLI edited the manuscript.

AUTHOR DISCLAIMER

Opinions, interpretations, conclusion, and recommendations are those of the author and are not necessarily endorsed by the Department of Defense.

CONFLICT OF INTEREST

The authors declare that the research was conducted in the absence of any commercial or financial relationships that could be construed as a potential conflict of interest.

REFERENCES

1. Breakefield XO, Blood AJ, Li Y, Hallett M, Hanson PI, Standaert DG, et al. The Pathophysiological Basis of Dystonias. *Nat Rev Neurosci* (2008) 9:222–34. doi:10.1038/nrn2337

2. Albanese A, Bhatia K, Bressman SB, Delong MR, Fahn S, Fung VS, et al. Phenomenology and Classification of Dystonia: A Consensus Update. *Mov Disord* (2013) 28:863–73. doi:10.1002/mds.25475

3. Ozelius LJ, Hewett JW, Page CE, Bressman SB, Kramer PL, Shalish C, et al. The Early-Onset Torsion Dystonia Gene (DYT1) Encodes an ATP-Binding Protein. *Nat Genet* (1997) 17:40–8. doi:10.1038/ng0997-40

4. Ghilardi MF, Carbon M, Silvestri G, Dhawan V, Tagliati M, Bressman S, et al. Impaired Sequence Learning in Carriers of the DYT1 Dystonia Mutation. *Ann Neurol* (2003) 54:102–9. doi:10.1002/ana.10610

5. Carbon M, Argyelan M, Ghilardi MF, Mattis P, Dhawan V, Bressman S, et al. Impaired Sequence Learning in Dystonia Mutation Carriers: A Genotypic Effect. *Brain* (2011) 134:1416–27. doi:10.1093/brain/awr060

6. Fahn S. High Dosage Anticholinergic Therapy in Dystonia. *Neurology* (1983) 33:1255–61. doi:10.1212/wnl.33.10.1255

7. Jankovic J. Treatment of Dystonia. *Lancet Neurol* (2006) 5:864–72. doi:10.1016/S1474-4422(06)70574-9

8. Dang MT, Yokoi F, McNaught KS, Jengelley TA, Jackson T, Li J, et al. Generation and Characterization of Dyt1 DeltaGAG Knock-In Mouse as a Model for Early-Onset Dystonia. *Exp Neurol* (2005) 196:452–63. doi:10.1016/j.expneurol.2005.08.025

9. Goodchild RE, Kim CE, Dauer WT. Loss of the Dystonia-Associated Protein torsinA Selectively Disrupts the Neuronal Nuclear Envelope. *Neuron* (2005) 48:923–32. doi:10.1016/j.neuron.2005.11.010

10. Yokoi F, Dang MT, Li Y. Improved Motor Performance in Dyt1 ΔGAG Heterozygous Knock-In Mice by Cerebellar Purkinje-Cell Specific Dyt1 Conditional Knocking-Out. *Behav Brain Res* (2012) 230:389–98. doi:10.1016/j.bbr.2012.02.029

11. Cao S, Hewett JW, Yokoi F, Lu J, Buckley AC, Burdette AJ, et al. Chemical Enhancement of torsinA Function in Cell and Animal Models of Torsion Dystonia. *Dis Model Mech* (2010) 3:386–96. doi:10.1242/dmm.003715

12. Song CH, Fan X, Exeter CJ, Hess EJ, Jinnah HA. Functional Analysis of Dopaminergic Systems in a DYT1 Knock-In Mouse Model of Dystonia. *Neurobiol Dis* (2012) 48:66–78. doi:10.1016/j.nbd.2012.05.009

13. Liu Y, Xing H, Yokoi F, Vaillancourt DE, Li Y. Investigating the Role of Striatal Dopamine Receptor 2 in Motor Coordination and Balance: Insights into the Pathogenesis of DYT1 Dystonia. *Behav Brain Res* (2021) 113137. doi:10.1016/j.bbr.2021.113137

14. Yokoi F, Dang MT, Li J, Li Y. Myoclonus, Motor Deficits, Alterations in Emotional Responses and Monoamine Metabolism in Epsilon-Sarcoglycan Deficient Mice. *J Biochem* (2006) 140:141–6. doi:10.1093/jb/mvj138

15. DeAndrade MP, Yokoi F, van Groen T, Lingrel JB, Li Y. Characterization of Atp1a3 Mutant Mice as a Model of Rapid-Onset Dystonia with Parkinsonism. *Behav Brain Res* (2011) 216:659–65. doi:10.1016/j.bbr.2010.09.009

16. Oleas J, Yokoi F, DeAndrade MP, Pisani A, Li Y. Engineering Animal Models of Dystonia. *Mov Disord* (2013) 28:990–1000. doi:10.1002/mds.25583

17. Oleas J, Yokoi F, DeAndrade MP, Li Y. Rodent Models of Autosomal Dominant Primary Dystonia. In: LeDoux MS, editor. *Movement Disorders: Genetics and Models*. New York: Academic Press Elsevier (2015). p. 483–505.

18. Imbriani P, Ponterio G, Tassone A, Sciamanna G, El Atiallah I, Bonsi P, et al. Models of Dystonia: An Update. *J Neurosci Methods* (2020) 339:108728. doi:10.1016/j.jneumeth.2020.108728

19. Richter F, Richter A. Genetic Animal Models of Dystonia: Common Features and Diversities. *Prog Neurobiol* (2014) 121:91–113. doi:10.1016/j.pneurobio.2014.07.002

20. Grundmann K, Glockle N, Martella G, Sciamanna G, Hauser TK, Yu L, et al. Generation of a Novel Rodent Model for DYT1 Dystonia. *Neurobiol Dis* (2012) 47:61–74. doi:10.1016/j.nbd.2012.03.024

21. Wakabayashi-Ito N, Ajjuri RR, Henderson BW, Doherty OM, Breakefield XO, O'Donnell JM, et al. Mutant Human torsinA, Responsible for Early-Onset Dystonia, Dominantly Suppresses GTPCH Expression, Dopamine Levels and Locomotion in *Drosophila melanogaster*. *Biol Open* (2015) 4:585–95. doi:10.1242/bio.201411080

22. Koh YH, Rehfeld K, Ganetzky B. A Drosophila Model of Early Onset Torsion Dystonia Suggests Impairment in TGF-β Signaling. *Hum Mol Genet* (2004) 13:2019–30. doi:10.1093/hmg/ddh208

23. Dang MT, Yokoi F, Cheetham CC, Lu J, Vo V, Lovinger DM, et al. An Anticholinergic Reverses Motor Control and Corticostriatal LTD Deficits in Dyt1 ΔGAG Knock-In Mice. *Behav Brain Res* (2012) 226:465–72. doi:10.1016/j.bbr.2011.10.002

24. DeAndrade MP, Trongnetrpunya A, Yokoi F, Cheetham CC, Peng N, Wyss JM, et al. Electromyographic Evidence in Support of a Knock-In Mouse Model of DYT1 Dystonia. *Mov Disord* (2016) 31:1633–9. doi:10.1002/mds.26677

25. Yokoi F, Dang MT, Liu J, Gandre JR, Kwon K, Yuen R, et al. Decreased Dopamine Receptor 1 Activity and Impaired Motor-Skill Transfer in Dyt1 ΔGAG Heterozygous Knock-In Mice. *Behav Brain Res* (2015) 279:202–10. doi:10.1016/j.bbr.2014.11.037

26. Yokoi F, Dang MT, Zhang L, Dexter KM, Efimenko I, Krishnaswamy S, et al. Reversal of Motor-Skill Transfer Impairment by Trihexyphenidyl and Reduction of Dorsolateral Striatal Cholinergic Interneurons in Dyt1 ΔGAG Knock-In Mice. *IBRO Neurosci Rep* (2021) 11:1–7. doi:10.1016/j.ibneur.2021.05.003

27. Giles LM, Chen J, Li L, Chin LS. Dystonia-associated Mutations Cause Premature Degradation of torsinA Protein and Cell-type-specific Mislocalization to the Nuclear Envelope. *Hum Mol Genet* (2008) 17:2712–22. doi:10.1093/hmg/ddn173

28. Gordon KL, Gonzalez-Alegre P. Consequences of the DYT1 Mutation on torsinA Oligomerization and Degradation. *Neuroscience* (2008) 157:588–95. doi:10.1016/j.neuroscience.2008.09.028

29. Dang MT, Yokoi F, Pence MA, Li Y. Motor Deficits and Hyperactivity in Dyt1 Knockdown Mice. *Neurosci Res* (2006) 56:470–4. doi:10.1016/j.neures.2006.09.005

30. Yokoi F, Chen HX, Dang MT, Cheetham CC, Campbell SL, Roper SN, et al. Behavioral and Electrophysiological Characterization of Dyt1 Heterozygous Knockout Mice. *PLoS One* (2015) 10:e0120916. doi:10.1371/journal.pone.0120916

31. Yokoi F, Dang MT, Mitsui S, Li J, Li Y. Motor Deficits and Hyperactivity in Cerebral Cortex-specific Dyt1 Conditional Knockout Mice. *J Biochem* (2008) 143:39–47. doi:10.1093/jb/mvm191

32. Jin XL, Guo H, Mao C, Atkins N, Wang H, Avasthi PP, et al. Emx1-specific Expression of Foreign Genes Using "Knock-In" Approach. *Biochem Biophys Res Commun* (2000) 270:978–82. doi:10.1006/bbrc.2000.2532

33. Yokoi F, Dang MT, Li J, Standaert DG, Li Y. Motor Deficits and Decreased Striatal Dopamine Receptor 2 Binding Activity in the Striatum-specific Dyt1 Conditional Knockout Mice. *PLoS One* (2011) 6:e24539. doi:10.1371/journal.pone.0024539

34. Dang MT, Yokoi F, Yin HH, Lovinger DM, Wang Y, Li Y, et al. Disrupted Motor Learning and Long-Term Synaptic Plasticity in Mice Lacking NMDAR1 in the Striatum. *Proc Natl Acad Sci U S A* (2006) 103:15254–9. doi:10.1073/pnas.0601758103

35. Sciamanna G, Hollis R, Ball C, Martella G, Tassone A, Marshall A, et al. Cholinergic Dysregulation Produced by Selective Inactivation of the Dystonia-Associated Protein torsinA. *Neurobiol Dis* (2012) 47:416–27. doi:10.1016/j.nbd.2012.04.015

36. Liu Y, Xing H, Sheng W, Singh KN, Korkmaz AG, Comeau C, et al. Alteration of the Cholinergic System and Motor Deficits in Cholinergic Neuron-specific Dyt1 Knockout Mice. *Neurobiol Dis* (2021) 154:105342. doi:10.1016/j.nbd.2021.105342

37. Yokoi F, Oleas J, Xing H, Liu Y, Dexter KM, Misztal C, et al. Decreased Number of Striatal Cholinergic Interneurons and Motor Deficits in Dopamine Receptor 2-expressing-cell-specific Dyt1 Conditional Knockout Mice. *Neurobiol Dis* (2020) 134:104638. doi:10.1016/j.nbd.2019.104638

38. Yokoi F, Chen HX, Oleas J, Dang MT, Xing H, Dexter KM, et al. Characterization of the Direct Pathway in Dyt1 ΔGAG Heterozygous Knock-In Mice and Dopamine Receptor 1-expressing-cell-specific Dyt1 Conditional Knockout Mice. *Behav Brain Res* (2021) 411:113381. doi:10.1016/j.bbr.2021.113381

39. Fremont R, Tewari A, Angueyra C, Khodakhah K. A Role for Cerebellum in the Hereditary Dystonia DYT1. *Elife* (2017) 6:e22775. doi:10.7554/eLife.22775

40. Shakkottai VG, Batla A, Bhatia K, Dauer WT, Dresel C, Niethammer M, et al. Current Opinions and Areas of Consensus on the Role of the Cerebellum in Dystonia. *Cerebellum* (2017) 16:577–94. doi:10.1007/s12311-016-0825-6

41. Yokoi F, Jiang F, Dexter K, Salvato B, Li Y. Improved Survival and Overt "dystonic" Symptoms in a torsinA Hypofunction Mouse Model. *Behav Brain Res* (2020) 381:112451. doi:10.1016/j.bbr.2019.112451

42. Liang CC, Tanabe LM, Jou S, Chi F, Dauer WT. TorsinA Hypofunction Causes Abnormal Twisting Movements and Sensorimotor Circuit Neurodegeneration. *J Clin Invest* (2014) 124:3080–92. doi:10.1172/JCI72830

43. Yokoi F, Cheetham CC, Campbell SL, Sweatt JD, Li Y. Pre-synaptic Release Deficits in a DYT1 Dystonia Mouse Model. *PLoS One* (2013) 8:e72491. doi:10.1371/journal.pone.0072491

44. Kakazu Y, Koh JY, Ho KW, Gonzalez-Alegre P, Harata NC. Synaptic Vesicle Recycling is Enhanced by torsinA that Harbors the DYT1 Dystonia Mutation. *Synapse* (2012) 66:453–64. doi:10.1002/syn.21534

45. Kakazu Y, Koh JY, Iwabuchi S, Gonzalez-Alegre P, Harata NC. Miniature Release Events of Glutamate from Hippocampal Neurons are Influenced by the Dystonia-Associated Protein torsinA. *Synapse* (2012) 66:807–22. doi:10.1002/syn.21571

46. Iwabuchi S, Kakazu Y, Koh JY, Harata NC. Abnormal Cytoplasmic Calcium Dynamics in central Neurons of a Dystonia Mouse Model. *Neurosci Lett* (2013) 548:61–6. doi:10.1016/j.neulet.2013.05.047

47. Pappas SS, Darr K, Holley SM, Cepeda C, Mabrouk OS, Wong JM, et al. Forebrain Deletion of the Dystonia Protein torsinA Causes Dystonic-like Movements and Loss of Striatal Cholinergic Neurons. *Elife* (2015) 4:e08352. doi:10.7554/eLife.08352

48. Sciamanna G, Tassone A, Martella G, Mandolesi G, Puglisi F, Cuomo D, et al. Developmental Profile of the Aberrant Dopamine D2 Receptor Response in Striatal Cholinergic Interneurons in DYT1 Dystonia. *PLoS One* (2011) 6:e24261. doi:10.1371/journal.pone.0024261

49. Martella G, Maltese M, Nistico R, Schirinzi T, Madeo G, Sciamanna G, et al. Regional Specificity of Synaptic Plasticity Deficits in a Knock-In Mouse Model of DYT1 Dystonia. *Neurobiol Dis* (2014) 65:124–32. doi:10.1016/j.nbd.2014.01.016

50. Ponterio G, Tassone A, Sciamanna G, Vanni V, Meringolo M, Santoro M, et al. Enhanced Mu Opioid Receptor-dependent Opioidergic Modulation of Striatal Cholinergic Transmission in DYT1 Dystonia. *Mov Disord* (2018) 33:310–20. doi:10.1002/mds.27212

51. Wilson CJ. The Mechanism of Intrinsic Amplification of Hyperpolarizations and Spontaneous Bursting in Striatal Cholinergic Interneurons. *Neuron* (2005) 45:575–85. doi:10.1016/j.neuron.2004.12.053

52. Bennett BD, Callaway JC, Wilson CJ. Intrinsic Membrane Properties Underlying Spontaneous Tonic Firing in Neostriatal Cholinergic Interneurons. *J Neurosci* (2000) 20:8493–503. doi:10.1523/jneurosci.20-22-08493.2000

53. Goldberg JA, Wilson CJ. Control of Spontaneous Firing Patterns by the Selective Coupling of Calcium Currents to Calcium-Activated Potassium Currents in Striatal Cholinergic Interneurons. *J Neurosci* (2005) 25:10230–8. doi:10.1523/JNEUROSCI.2734-05.2005

54. Goldberg JA, Teagarden MA, Foehring RC, Wilson CJ. Nonequilibrium Calcium Dynamics Regulate the Autonomous Firing Pattern of Rat Striatal Cholinergic Interneurons. *J Neurosci* (2009) 29:8396–407. doi:10.1523/JNEUROSCI.5582-08.2009

55. Mamaligas AA, Barcomb K, Ford CP. Cholinergic Transmission at Muscarinic Synapses in the Striatum Is Driven Equally by Cortical and Thalamic Inputs. *Cell Rep* (2019) 28:1003–14. doi:10.1016/j.celrep.2019.06.077

56. Straub C, Tritsch NX, Hagan NA, Gu C, Sabatini BL. Multiphasic Modulation of Cholinergic Interneurons by Nigrostriatal Afferents. *J Neurosci* (2014) 34:8557–69. doi:10.1523/JNEUROSCI.0589-14.2014

57. Chuhma N, Mingote S, Moore H, Rayport S. Dopamine Neurons Control Striatal Cholinergic Neurons via Regionally Heterogeneous Dopamine and Glutamate Signaling. *Neuron* (2014) 81:901–12. doi:10.1016/j.neuron.2013.12.027

58. Lim SA, Kang UJ, McGehee DS. Striatal Cholinergic Interneuron Regulation and Circuit Effects. *Front Synaptic Neurosci* (2014) 6:22. doi:10.3389/fnsyn.2014.00022

59. Suzuki E, Momiyama T. M1 Muscarinic Acetylcholine Receptor-Mediated Inhibition of GABA Release from Striatal Medium Spiny Neurons onto Cholinergic Interneurons. *Eur J Neurosci* (2021) 53:796–813. doi:10.1111/ejn.15074

60. Yan Z, Surmeier DJ. Muscarinic (M2/m4) Receptors Reduce N- and P-type Ca2+ Currents in Rat Neostriatal Cholinergic Interneurons through a Fast, Membrane-Delimited, G-Protein Pathway. *J Neurosci* (1996) 16:2592–604. doi:10.1523/jneurosci.16-08-02592.1996

61. Ding J, Guzman JN, Tkatch T, Chen S, Goldberg JA, Ebert PJ, et al. RGS4-dependent Attenuation of M4 Autoreceptor Function in Striatal Cholinergic Interneurons Following Dopamine Depletion. *Nat Neurosci* (2006) 9:832–42. doi:10.1038/nn1700

62. Howe AR, Surmeier DJ. Muscarinic Receptors Modulate N-P-And L-type Ca2+ Currents in Rat Striatal Neurons through Parallel Pathways. *J Neurosci* (1995) 15:458–69. doi:10.1523/jneurosci.15-01-00458.1995

63. Wang Z, Kai L, Day M, Ronesi J, Yin HH, Ding J, et al. Dopaminergic Control of Corticostriatal Long-Term Synaptic Depression in Medium Spiny Neurons is Mediated by Cholinergic Interneurons. *Neuron* (2006) 50:443–52. doi:10.1016/j.neuron.2006.04.010

64. Yan Z, Flores-Hernandez J, Surmeier DJ. Coordinated Expression of Muscarinic Receptor Messenger RNAs in Striatal Medium Spiny Neurons. *Neuroscience* (2001) 103:1017–24. doi:10.1016/s0306-4522(01)00039-2

65. Richter F, Klein L, Helmschrodt C, Richter A. Subtle Changes in Striatal Muscarinic M1 and M4 Receptor Expression in the DYT1 Knock-In Mouse Model of Dystonia. *PLoS One* (2019) 14:e0226080. doi:10.1371/journal.pone.0226080

66. Mamaligas AA, Ford CP. Spontaneous Synaptic Activation of Muscarinic Receptors by Striatal Cholinergic Neuron Firing. *Neuron* (2016) 91:574–86. doi:10.1016/j.neuron.2016.06.021

67. Threlfell S, Lalic T, Platt NJ, Jennings KA, Deisseroth K, Cragg SJ, et al. Striatal Dopamine Release is Triggered by Synchronized Activity in Cholinergic Interneurons. *Neuron* (2012) 75:58–64. doi:10.1016/j.neuron.2012.04.038

68. Maurice N, Mercer J, Chan CS, Hernandez-Lopez S, Held J, Tkatch T, et al. D2 Dopamine Receptor-Mediated Modulation of Voltage-dependent Na+ Channels Reduces Autonomous Activity in Striatal Cholinergic Interneurons. *J Neurosci* (2004) 24:10289–301. doi:10.1523/JNEUROSCI.2155-04.2004

69. Yokoi F, Dang MT, Miller CA, Marshall AG, Campbell SL, Sweatt JD, et al. Increased C-Fos Expression in the central Nucleus of the Amygdala and Enhancement of Cued Fear Memory in Dyt1 DeltaGAG Knock-In Mice. *Neurosci Res* (2009) 65:228–35. doi:10.1016/j.neures.2009.07.004

70. Voelkl B, Altman NS, Forsman A, Forstmeier W, Gurevitch J, Jaric I, et al. Reproducibility of Animal Research in Light of Biological Variation. *Nat Rev Neurosci* (2020) 21:384–93. doi:10.1038/s41583-020-0313-3

71. Lyu S, Xing H, DeAndrade MP, Liu Y, Perez PD, Yokoi F, et al. The Role of BTBD9 in Striatum and Restless Legs Syndrome. *eNeuro* (2019) 6:ENEURO.0277-19.2019. doi:10.1523/ENEURO.0277-19.2019

72. Lyu S, Xing H, Liu Y, Girdhar P, Zhang K, Yokoi F, et al. Deficiency of Meis1, a Transcriptional Regulator, in Mice and Worms: Neurochemical and Behavioral Characterizations with Implications in the Restless Legs Syndrome. *J Neurochem* (2020) 155:522–37. doi:10.1111/jnc.15177

73. Bennett BD, Wilson CJ. Spontaneous Activity of Neostriatal Cholinergic Interneurons *In Vitro*. *J Neurosci* (1999) 19:5586–96. doi:10.1523/jneurosci.19-13-05586.1999

74. Sholl DA. Dendritic Organization in the Neurons of the Visual and Motor Cortices of the Cat. *J Anat* (1953) 87:387–406.

75. Student. The Probable Error of a Mean. *Biometrika* (1908) 6:1. doi:10.2307/2331554

76. Eskow Jaunarajs KL, Bonsi P, Chesselet MF, Standaert DG, Pisani A. Striatal Cholinergic Dysfunction as a Unifying Theme in the Pathophysiology of Dystonia. *Prog Neurobiol* (2015) 127-128:91–107. doi:10.1016/j.pneurobio.2015.02.002

77. Bonsi P, Ponterio G, Vanni V, Tassone A, Sciamanna G, Migliarini S, et al. RGS9-2 Rescues Dopamine D2 Receptor Levels and Signaling in DYT1 Dystonia Mouse Models. *EMBO Mol Med* (2019) 11:e9283. doi:10.15252/emmm.201809283

78. Caffall ZF, Wilkes BJ, Hernández-Martinez R, Rittiner JE, Fox JT, Wan KK, et al. The HIV Protease Inhibitor, Ritonavir, Corrects Diverse Brain Phenotypes across Development in Mouse Model of DYT-TOR1A Dystonia. *Sci Transl Med* (2021) 13:eabd3904. doi:10.1126/scitranslmed.abd3904

79. Scarduzio M, Zimmerman CN, Jaunarajs KL, Wang Q, Standaert DG, McMahon LL, et al. Strength of Cholinergic Tone Dictates the Polarity of Dopamine D2 Receptor Modulation of Striatal Cholinergic Interneuron Excitability in DYT1 Dystonia. *Exp Neurol* (2017) 295:162–75. doi:10.1016/j.expneurol.2017.06.005

80. Oswald MJ, Oorschot DE, Schulz JM, Lipski J, Reynolds JN. IH Current Generates the Afterhyperpolarisation Following Activation of Subthreshold Cortical Synaptic Inputs to Striatal Cholinergic Interneurons. *J Physiol* (2009) 587:5879–97. doi:10.1113/jphysiol.2009.177600

81. Zhang L, Zhang JT, Hang L, Liu T. Mu Opioid Receptor Heterodimers Emerge as Novel Therapeutic Targets: Recent Progress and Future Perspective. *Front Pharmacol* (2020) 11:1078. doi:10.3389/fphar.2020.01078

82. Ponterio G, Tassone A, Sciamanna G, Riahi E, Vanni V, Bonsi P, et al. Powerful Inhibitory Action of Mu Opioid Receptors (MOR) on Cholinergic Interneuron Excitability in the Dorsal Striatum. *Neuropharmacology* (2013) 75:78–85. doi:10.1016/j.neuropharm.2013.07.006

83. Brelidze TI, Niu X, Magleby KL. A Ring of Eight Conserved Negatively Charged Amino Acids Doubles the Conductance of BK Channels and Prevents Inward Rectification. *Proc Natl Acad Sci U S A* (2003) 100:9017–22. doi:10.1073/pnas.1532257100

84. Carvacho I, Gonzalez W, Torres YP, Brauchi S, Alvarez O, Gonzalez-Nilo FD, et al. Intrinsic Electrostatic Potential in the BK Channel Pore: Role in Determining Single Channel Conductance and Block. *J Gen Physiol* (2008) 131:147–61. doi:10.1085/jgp.200709862

85. Tsantoulas C, McMahon SB. Opening Paths to Novel Analgesics: The Role of Potassium Channels in Chronic Pain. *Trends Neurosci* (2014) 37:146–58. doi:10.1016/j.tins.2013.12.002

86. Gonzalez-Alegre P. Advances in Molecular and Cell Biology of Dystonia: Focus on torsinA. *Neurobiol Dis* (2019) 127:233–41. doi:10.1016/j.nbd.2019.03.007

87. Eskow Jaunarajs KL, Scarduzio M, Ehrlich ME, McMahon LL, Standaert DG. Diverse Mechanisms Lead to Common Dysfunction of Striatal Cholinergic Interneurons in Distinct Genetic Mouse Models of Dystonia. *J Neurosci* (2019) 39:7195–205. doi:10.1523/JNEUROSCI.0407-19.2019

88. Grundmann K, Reischmann B, Vanhoutte G, Hubener J, Teismann P, Hauser TK, et al. Overexpression of Human Wildtype torsinA and Human

DeltaGAG torsinA in a Transgenic Mouse Model Causes Phenotypic Abnormalities. *Neurobiol Dis* (2007) 27:190–206. doi:10.1016/j.nbd.2007.04.015

89. Whone AL, Von Spiczak S, Edwards M, Valente EM, Hammers A, Bhatia KP, et al. Opioid Binding in DYT1 Primary Torsion Dystonia: An 11C-Diprenorphine PET Study. *Mov Disord* (2004) 19:1498–503. doi:10.1002/mds.20238

90. Pham P, Frei KP, Woo W, Truong DD. Molecular Defects of the Dystonia-Causing torsinA Mutation. *Neuroreport* (2006) 17:1725–8. doi:10.1097/WNR.0b013e3280101220

91. Gonzales KK, Smith Y. Cholinergic Interneurons in the Dorsal and Ventral Striatum: Anatomical and Functional Considerations in normal and Diseased Conditions. *Ann N Y Acad Sci* (2015) 1349:1–45. doi:10.1111/nyas.12762

92. Gonzales KK, Pare JF, Wichmann T, Smith Y. GABAergic Inputs from Direct and Indirect Striatal Projection Neurons onto Cholinergic Interneurons in the Primate Putamen. *J Comp Neurol* (2013) 521:2502–22. doi:10.1002/cne.23295

93. van Harten PN, Hoek HW, Kahn RS. Acute Dystonia Induced by Drug Treatment. *BMJ* (1999) 319:623–6. doi:10.1136/bmj.319.7210.623

94. Ichinose H, Ohye T, Takahashi E, Seki N, Hori T, Segawa M, et al. Hereditary Progressive Dystonia with Marked Diurnal Fluctuation Caused by Mutations in the GTP Cyclohydrolase I Gene. *Nat Genet* (1994) 8:236–42. doi:10.1038/ng1194-236

95. Torres GE, Sweeney AL, Beaulieu JM, Shashidharan P, Caron MG. Effect of torsinA on Membrane Proteins Reveals a Loss of Function and a Dominant-Negative Phenotype of the Dystonia-Associated DeltaE-torsinA Mutant. *Proc Natl Acad Sci U S A* (2004) 101:15650–5. doi:10.1073/pnas.0308088101

96. Yokoi F, Yang G, Li J, DeAndrade MP, Zhou T, Li Y, et al. Earlier Onset of Motor Deficits in Mice with Double Mutations in Dyt1 and Sgce. *J Biochem* (2010) 148:459–66. doi:10.1093/jb/mvq078

97. Liu Y, Xing H, Wilkes BJ, Yokoi F, Chen H, Vaillancourt DE, et al. The Abnormal Firing of Purkinje Cells in the Knockin Mouse Model of DYT1 Dystonia. *Brain Res Bull* (2020) 165:14–22. doi:10.1016/j.brainresbull.2020.09.011

98. Dawson VL, Dawson TM, Wamsley JK. Muscarinic and Dopaminergic Receptor Subtypes on Striatal Cholinergic Interneurons. *Brain Res Bull* (1990) 25:903–12. doi:10.1016/0361-9230(90)90186-4

99. Alcantara AA, Mrzljak L, Jakab RL, Levey AI, Hersch SM, Goldman-Rakic PS, et al. Muscarinic M1 and M2 Receptor Proteins in Local Circuit and Projection Neurons of the Primate Striatum: Anatomical Evidence for Cholinergic Modulation of Glutamatergic Prefronto-Striatal Pathways. *J Comp Neurol* (2001) 434:445–60. doi:10.1002/cne.1186

100. Rittiner JE, Caffall ZF, Hernández-Martinez R, Sanderson SM, Pearson JL, Tsukayama KK, et al. Functional Genomic Analyses of Mendelian and Sporadic Disease Identify Impaired eIF2α Signaling as a Generalizable Mechanism for Dystonia. *Neuron* (2016) 92:1238–51. doi:10.1016/j.neuron.2016.11.012

101. Zhang L, Yokoi F, Jin YH, Deandrade MP, Hashimoto K, Standaert DG, et al. Altered Dendritic Morphology of Purkinje Cells in Dyt1 ΔGAG Knock-In and Purkinje Cell-specific Dyt1 Conditional Knockout Mice. *PLoS One* (2011) 6:e18357. doi:10.1371/journal.pone.0018357

102. Song CH, Bernhard D, Hess EJ, Jinnah HA. Subtle Microstructural Changes of the Cerebellum in a Knock-In Mouse Model of DYT1 Dystonia. *Neurobiol Dis* (2014) 62:372–80. doi:10.1016/j.nbd.2013.10.003

103. Song CH, Bernhard D, Bolarinwa C, Hess EJ, Smith Y, Jinnah HA, et al. Subtle Microstructural Changes of the Striatum in a DYT1 Knock-In Mouse Model of Dystonia. *Neurobiol Dis* (2013) 54:362–71. doi:10.1016/j.nbd.2013.01.008